Scanning Electrochemical Microscopy of Redox-Mediated Hydrogen Evolution Catalyzed by Two-Dimensional Assemblies of Palladium Nanoparticles

7 AUTHORS, INCLUDING:

Paolo Bertoncello
Swansea University
41 PUBLICATIONS **1,269** CITATIONS

David J. Fermín
University of Bristol
111 PUBLICATIONS **1,844** CITATIONS

Scanning Electrochemical Microscopy of Redox-Mediated Hydrogen Evolution Catalyzed by Two-Dimensional Assemblies of Palladium Nanoparticles

Fei Li,[†] **Ilenia Ciani,**[†] **Paolo Bertoncello,**[†] **Patrick R. Unwin,**[*,†] **Jianjun Zhao,**[‡] **Christopher R. Bradbury,**[‡] **and David J. Fermin**[*,‡]

Department of Chemistry, University of Warwick, Coventry CV4 7AL, United Kingdom, and Department of Chemistry and Biochemistry, University of Berne, Freiestrasse 3, Berne, CH-3012, Switzerland

Received: January 7, 2008; Revised Manuscript Received: March 24, 2008

The kinetics of the hydrogen evolution reaction (HER) catalyzed by two-dimensional assemblies of 13 nm diameter palladium (Pd) nanoparticles on mica substrates was investigated by scanning electrochemical microscopy (SECM). The assemblies were prepared by electrostatic adsorption of citrate-stabilized Pd nanoparticles on poly-L-lysine treated mica. Atomic force microscopy (AFM) studies of the adsorption process provided information on the nanoparticle number density as a function of the adsorption time. The HER kinetics was determined by examining SECM feedback approach curves, employing the methyl viologen $(MV^{2+/+\bullet})$ couple as the redox probe. With this configuration, the potential of the Pd nanoparticles is effectively determined by the local concentration ratio of the redox probe. The overpotential for proton reduction can be finely tuned by the concentration of the redox species, the size of the ultramicroelectrode (UME) tip, and the distance between the UME and the nanoparticle assembly. The SECM analysis allowed the mean exchange current density per Pd nanoparticle $[j_{0(pH = 3)} = (1.19 \pm 0.08) \times 10^{-6} \text{ A cm}^{-2}]$ to be evaluated. Significantly, the SECM methodology described is highly sensitive to the transfer coefficient of the HER, with a value of 0.5 providing the most satisfactory fit in the overpotential range investigated. It is concluded that the reactivity of the Pd nanoparticles is comparable to the bulk metal, which is consistent with the bulk-like electronic structure of Pd clusters of this dimension.

1. Introduction

The electrochemical hydrogen evolution reaction (HER) is topical in terms of both fundamental interest and in the context of efficient hydrogen generation for energy applications.[1–10] In recent years, research into new materials for cathodes has shifted from bulk materials[11] to nanomaterials supported at electrode surfaces.[12–18] The ability to manipulate not only the size but also the shape of nanocrystals has led to the observation of unusual catalytic activity.[19] Of particular relevance to the HER of interest, herein, is the modification of electrode surfaces with Pd nanoparticles, which has received some recent attention.[6,9,15b,20–23]

The HER on bulk metals, such as platinum, palladium, and rhodium in acidic solution, has been the subject of a number of classical mechanistic studies.[24–29] More recently, Nørskov and co-workers have related the electrocatalytic properties of Pd and other materials to H-adsorption energies calculated from density functional theory (DFT).[30] Although qualitative correlations with experimental results appeared to validate this theoretical approach, Schmickler and Trasatti have pointed out rather fundamental short-comings.[31] Another controversial issue has arisen from the interpretation of the enhancement of the electrocatalytic activity of Pd clusters with decreasing size on gold (Au) (111) surfaces.[20,32] These outstanding issues require the development of in situ experimental techniques which can address the intrinsic catalytic activity of Pd nanoparticles, free from electronic effects of the supporting surface.

Scanning electrochemical microscopy (SECM) has been used to study surface processes relevant to electrocatalysis and fuel cells.[33–41] This method has proven highly sensitive to the measurement of fast kinetics and for the development of combinatorial and rapid screening approaches for assessing catalysts. More generally, SECM is proving powerful for investigating the kinetics of various processes in nanostructured materials.[42–46] Previous studies by Zhang et al. demonstrated that SECM is a sensitive "contactless" method for inducing and monitoring HER kinetics on gold nanoparticles,[36] building on earlier work on microscale interfaces.[33]

In this paper, SECM has been employed to investigate the kinetics and mechanism of the HER catalyzed by Pd nanoparticles on an inert support with the methyl viologen $(MV^{2+/+\bullet})$ couple as the redox probe. We investigated the effect of the number density of nanoparticles on the support, which was controlled via electrostatic adsorption.[47–50] This method of immobilization has proven a convenient and versatile approach to control a variety of two-dimensional (2D) and three-dimensional (3D) nanostructured assemblies.[47,49,51,52] In our studies, information on the nanoparticle number density, as a function of the adsorption time, was obtained by atomic force microscopy (AFM) studies of the adsorption process. Quantification of the HER kinetics as a function of the nanoparticle number density allowed the average exchange current density for a single nanoparticle to be determined. We also show that SECM feedback approach curves are sensitive to the potential dependence of the HER kinetics, from which the transfer coefficient can be determined accurately.

* Corresponding author. Phone: +44 (0) 2476 523264. Fax: +44 (0) 2476 524112. E-mail: p.r.unwin@warwick.ac.uk (P.R.U.). Phone: +44 (0) 1179 288981. Fax: +44 (0) 1179 250612. E-mail: David.Fermin@bristol.ac.uk (D.J.F.).
† University of Warwick.
‡ University of Berne.

Redox-Mediated Hydrogen Evolution

J. Phys. Chem. C, Vol. 112, No. 26, 2008 **9687**

2. Experimental Section

2.1. Chemicals and Solutions. Sodium hexachloropalladate (IV) tetrahydrate ($Na_2PdCl_6\cdot4H_2O$, 99%) and sodium citrate dihydrate ($C_6H_5Na_3O_7\cdot2H_2O$, 99%) were purchased from Sigma-Aldrich. Methyl viologen dichloride hydrate (MV-$Cl_2\cdot xH_2O$, Acros, 98%) and KNO_3 (Fisher, analytical grade) were used as the redox mediator and base electrolyte, respectively, in the solution. The pH 3 buffered solution for the SECM experiments was prepared using potassium hydrogen phthalate (Aldrich) and HCl (BDH, AnalaR) and contained 0.1 mM MV^{2+} and 0.1 M KNO_3. Poly-L-lysine solution (PLYS, 0.1% w/v, in water, trimerosal, 0.01%, added as preservative) and hexaamineruthenium (III) chloride ($Ru(NH_3)_6Cl_3$, 99%) were purchased from Sigma-Aldrich and Strem Chemicals, respectively. Solutions for electrodepositing mercury on a gold ultramicroelectrode (UME) consisted of 10 mM $Hg_2(NO_3)_2$ (Fisons, p.a.), 0.5 M KNO_3, and 1% HNO_3 (BDH, AnalaR). All chemicals were used as received. Solutions were prepared from Milli-Q reagent water (Millipore Corp., resistivity 18.2 MΩ/cm at 25 °C).

2.2. Synthesis of Pd Nanoparticles. Citrate-stabilized Pd nanoparticles were prepared by reduction of $PdCl_6^{2-}$ in the presence of citrate.[53] In this procedure, 20.17 mg of $Na_2PdCl_6\cdot4H_2O$ was dissolved in 150 cm^3 of Milli-Q water, then heated to boiling point, and kept under reflux. Subsequently, 18 cm^3 of 0.1% (wt) sodium citrate solution was injected into the refluxing Na_2PdCl_6 solution. The reaction was stopped after 4 h by allowing the solution to cool down to room temperature under reflux and with vigorous stirring. The particle size was estimated by height histograms of acoustic AFM images of low coverage 2D arrays on PLYS-modified mica surfaces. The average particle diameter was 13.0 ± 3.3 nm.

2.3. Electrostatic Assembly of Pd Nanoparticle Arrays. Citrate-stabilized Pd nanoparticles were adsorbed on PLYS-treated mica (Quality grade V1, BAL-TEC, Liechtenstein) by electrostatic interaction. Mica surfaces were freshly cleaved just before use and were functionalized by immersion in an unbuffered solution of PLYS (1 mg cm^{-3}) for 30 min, followed by copious rinsing with Milli-Q water. This step generated an ultrathin film of the polycation, which covered the surface. As shown below, electrostatic adsorption of the Pd nanoparticles on PLYS films was found to be a rather convenient way to control the nanoparticle number density on the support. This was achieved by dipping the freshly prepared PLYS-treated mica into the colloidal Pd solution for a period ranging between 1 min and 1 h. After removing the mica from the nanoparticle solution, the surface was rinsed further with Milli-Q water and dried in a stream of pure nitrogen.

2.4. SECM Tip. A 25 μm base diameter Au/Hg UME (*RG* = 10, the ratio of the overall tip radius to that of the gold microdisk) with an oblate hemispheroid shape (see below) was employed as the SECM tip for two reasons. First, mercury enhances the potential window in the cathodic region in aqueous solution, which is advantageous for the reduction of MV^{2+}. Second, the UME protrudes beyond the plane of the glass sheath, so allowing intimate contact between the electrode and surface in approach curve measurements, which is desirable for the accurate determination of tip−substrate separations.

The fabrication of the Au/Hg UME followed the procedure reported previously,[54–56] in which mercury was electrodeposited on the metal microdisk from a deaerated mercurous ion salt solution.[54,55] The shape of the resulting mercury layer formed on the surface of the gold microdisk was observed using an optical microscope (Olym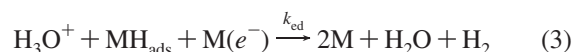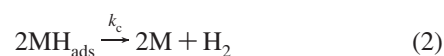pus BH2 microscope) as an oblate hemispheroid, characterized by a height, which was half-that of the disk radius. The electrochemical stability and the geometry of the Au/Hg UME were further validated by measuring the diffusion-limited current for the reduction of oxygen and $Ru(NH_3)_6^{3+}$ (separately) in aqueous solutions under steady-state conditions.[54,55] Before experiments, the Au/Hg UME was stored in a 0.1 M KNO_3 solution and carefully washed with copious amounts of Milli-Q water.

2.5. Electrochemical Measurements. Voltammetric measurements were made with a 730A electrochemical analyzer (CH Instruments). The SECM apparatus was homemade and has been described in detail previously.[57] The electrode configuration is illustrated in Figure 1, featuring a Au/Hg UME as the SECM tip and a silver quasi-reference electrode, AgQRE. A PLYS-treated mica substrate with adsorbed Pd nanoparticles was placed in the base of a Teflon cell and used as the substrate for the SECM measurements. The Au/Hg UME was typically held a potential of −0.9 V versus AgQRE, where the reduction of MV^{2+} to $MV^{+\bullet}$ was driven at a diffusion-controlled rate. Approach curves of steady-state diffusion-limited current as a function of distance, *d*, of the UME from the substrate were recorded by translating the probe toward the surface at a velocity of 0.5 μm s^{-1}. For each experimental condition, approach curves were measured at more than six different spots on the substrate to ensure reproducibility. All of the experiments were carried out under a nitrogen atmosphere at a temperature of 22 °C in an air-conditioned room.

2.6. AFM Measurements. Topographic images of Pd nanoparticle arrays were obtained with ex-situ AFM measurements in acoustic mode (PicoLE, Molecular Imaging). The PPP-NCH AFM tips (Nanosensors) used in these experiments typically exhibited a radius of curvature below 10 nm, 42 N/m force constant, and 300 kHz resonance frequency. The average particle size quoted earlier was estimated from statistical analysis of particle height in samples with a low number density of Pd nanoparticles on PLYS-treated mica surfaces.

3. Theory and Simulations

3.1. Mechanistic Models. Previous studies of the HER on electrode surfaces in acid solutions have invoked the following steps:[58]

$$H_3O^+ + M(e^-) \xrightarrow{k_d} MH_{ads} + H_2O \qquad (1)$$

$$2MH_{ads} \xrightarrow{k_c} 2M + H_2 \qquad (2)$$

$$H_3O^+ + MH_{ads} + M(e^-) \xrightarrow{k_{ed}} 2M + H_2O + H_2 \qquad (3)$$

where M represents a metal atom of the electrode, MH_{ads} is an adsorbed hydrogen atom on the metal surface, k_d, k_c, and k_{ed} are the rate constants of the discharge, chemical-desorption, and electrodic-desorption steps, respectively. Two basic reaction paths of the HER are regarded as likely: a primary discharge step (eq 1) followed by either chemical-desorption (eq 2) or electrodic-desorption (eq 3). These two pathways are termed the Volmer−Tafel and Volmer−Heyrovsky mechanisms, respectively. If discharge is the rate-determining step (RDS), the amount of adsorbed hydrogen on the metal surface tends to be low since the adsorbed hydrogen atoms generated in this step react and are desorbed swiftly. If desorption is the RDS, hydrogen atoms accumulate at the surface.[58]

In the Volmer–Tafel mechanism, taking the discharge-step (1) as the RDS, the current density (j) is given by the Butler–Volmer equation

$$j = 2Fk_d c_{H^+}(1 - \theta) \exp\left(-\frac{\beta F}{RT}\eta\right) \quad (4)$$

where c_{H^+} is the concentration of H$^+$, θ is the fraction of the surface covered with adsorbed hydrogen, η is overpotential, and β is the symmetry factor. Since the discharge step determines the overall reaction rate, the coverage of adsorbed hydrogen on the surface is low ($\theta \to 0$). Consequently, eq 4 can be written as

$$j = 2Fk_d c_{H^+} \exp\left(-\frac{\beta F}{RT}\eta\right) \quad (5)$$

In this case, the phenomenological transfer coefficient α is equal to the symmetry factor; that is, $\alpha = \beta = 0.5$.

If the discharge step is in equilibrium and followed by a rate-determining chemical-desorption step, the electronation-current density is expressed by

$$j = 2Fk_c(N_H\theta)^2 \quad (6)$$

where N_H is the quantity of adsorbed hydrogen atoms at maximum surface coverage (mol cm^{-2}). When the discharge step is in a quasi-equilibrium and the overpotential is low, θ is given by[58]

$$\theta \approx \frac{k_d c_{H^+} \exp\left(-\frac{F\eta}{RT}\right)}{k_{-d}N_{H^+}} \quad (7)$$

where k_{-d} is the rate constant for the back reaction of the discharge step. By combining eq 6 and eq 7,

$$j = 2Fk_c\left(\frac{k_d}{k_{-d}}\right)^2 (c_{H^+})^2 \exp\left(-\frac{2F\eta}{RT}\right) \quad (8)$$

Thus, the value of α for a discharge step in quasi-equilibrium followed by rate-determining chemical-desorption is 2.

The Volmer–Heyrovsky mechanism is often applicable at high overpotentials. Akin to the Volmer–Tafel mechanism, for a discharge–rate determining process followed by electrodic-desorption, $\alpha = 0.5$, while for discharge followed by rate determining electrodic-desorption, $\alpha = 1.5$.[58] As summarized in Table 10.13 in ref 58, the value of α can provide considerable mechanistic information. However, it should be noted that $\alpha = 0.5$ arises from four different mechanisms.[58] Therefore, the determination of the transfer coefficient alone may not provide a unique mechanistic interpretation but can provide insight. Clearly, the mechanism depends on parameters such as the overpotential, which need to be considered to provide a more complete mechanistic understanding.

3.2. Description of the SECM Numerical Model. Figure 1a illustrates the SECM feedback mode[41] implemented in this study. A tip UME positioned in the vicinity of a substrate surface is translated slowly toward the substrate while generating the reductant, MV$^{+\bullet}$, from the diffusion-limited reduction of MV^{2+}, present in bulk solution. MV$^{+\bullet}$ may inject an electron into a Pd nanoparticle to catalyze the reduction of protons to hydrogen, regenerating MV^{2+} at the substrate, which is detected at the tip (diffusional feedback). By measuring the tip current as a function of d (approach curve), information on the local kinetics of H$_2$ evolution can be obtained. In essence, the concentration ratio of MV^{2+}/MV$^{+\bullet}$ at the nanoparticle-modified surface controls
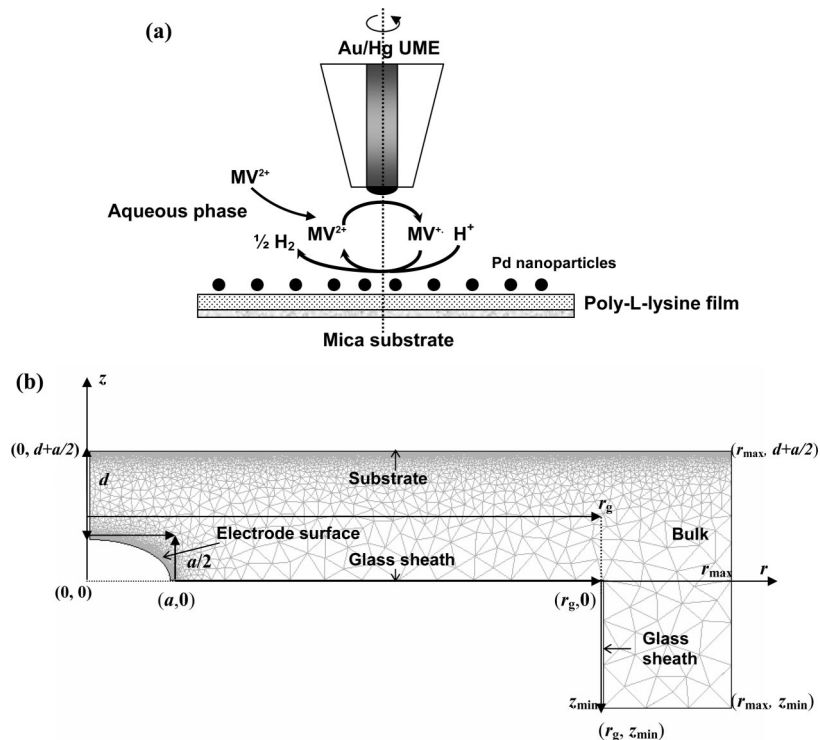

Figure 1. Schematics of (a) the SECM experimental arrangement (not to scale) for probing the HER catalyzed by citrate-stabilized Pd nanoparticles adsorbed on a PLYS-treated mica surface and (b) the SECM axisymmetric cylindrical geometry and coordinate system used for the simulations (not to scale). The coordinates r and z are measured from the center of the UME in the radial and normal directions, respectively. The UME is characterized by a base electrode radius, a, maximum height, $a/2$, and r_g is the distance from the center of the electrode to the edge of the surrounding insulating glass sheath. The parameters d, r_{max}, and z_{min} respectively denote the distance between the mica substrate and the surface of the mercury layer on the electrode, the maximum value in the r direction, and the minimum value in the z direction, for the selected domain.

Redox-Mediated Hydrogen Evolution

J. Phys. Chem. C, Vol. 112, No. 26, 2008 **9689**

the Fermi level of the nanoparticles, thereby controlling the driving force for the HER.

The geometry and coordinate system, together with a representation of the type of grid used for finite element simulations, are illustrated in Figure 1b. An axisymmetric cylindrical two-dimensional domain describes the simulation of interest. To simplify the problem, the diffusion coefficients of MV^{2+} and $MV^{+\bullet}$ have been considered to be equivalent;[36] that is, $D_{MV^{2+}} = D_{MV^{+\bullet}}$, which is a good assumption. This allows the principle of mass conservation to be invoked on the interior of the domain:

$$c_{MV^{2+}}(r, z) = c_{MV^{2+}}^* - c_{MV^{+\bullet}}(r, z) \quad (9)$$

where $c_{MV^{2+}}(r,z)$ and $c_{MV^{+\bullet}}(r,z)$ are the spatial-dependent concentrations of MV^{2+} and $MV^{+\bullet}$, defined in terms of r and z, which are the coordinates in the radial and normal directions, respectively, relative to the electrode surface, with the center as the origin. $c_{MV^{2+}}^*$ is the concentration of MV^{2+} in the bulk solution.

The diffusion equation, under steady-state conditions, in axisymmetric cylindrical coordinates is

$$D_{MV^{2+}}\left[\frac{\partial^2 c_{MV^{2+}}(r, z)}{\partial r^2} + \frac{1}{r}\frac{\partial c_{MV^{2+}}(r, z)}{\partial r} + \frac{\partial^2 c_{MV^{2+}}(r, z)}{\partial z^2}\right] = 0 \quad (10)$$

To calculate the tip current response, eq 10 was solved subject to the following boundary conditions:

$$0 < r \le a, \ z = \frac{1}{2}\sqrt{a^2 - r^2}: \ c_{MV^{2+}}(r, z) = 0 \quad (11)$$

$$a < r \le r_g, \ z = 0: \ D_{MV^{2+}}\frac{\partial c_{MV^{2+}}(r, z)}{\partial z} = 0 \quad (12)$$

$$r = r_g, \ 0 < z \le z_{min}: \ D_{MV^{2+}}\frac{\partial c_{MV^{2+}}(r, z)}{\partial r} = 0 \quad (13)$$

$$r_g < r < r_{max}, \ z = z_{min}: \ c_{MV^{2+}}(r, z) = c_{MV^{2+}}^* \quad (14)$$

$$r = r_{max}, \ z_{min} < z \le \left(d + \frac{a}{2}\right): \ c_{MV^{2+}}(r, z) = c_{MV^{2+}}^* \quad (15)$$

$$r = 0, \ \frac{a}{2} \le z \le \left(d + \frac{a}{2}\right): \ D_{MV^{2+}}\frac{\partial c_{MV^{2+}}(r, z)}{\partial r} = 0 \quad (16)$$

where the parameters a, d, r_{max}, and z_{min} respectively denote the base electrode radius, distance between the substrate and the surface of the mercury layer on the electrode, the maximum value in the r direction, and the minimum value in the z direction for the selected domain. The parameter r_g is the radial distance from the axis of symmetry to the edge of the insulating glass sheath surrounding the electrode, which was typically $10a$ for the studies herein.

The boundary conditions relate to the following: the potential of the UME surface is set at a value to drive the reduction of MV^{2+} at a diffusion-controlled rate (eq 11). The concentration of MV^{2+} is assumed to be unaltered by the insulating glass sheath (eq 12 and eq 13) and to remain at bulk concentration values on the edge of the domain (eq 14 and eq 15). Equation 16 follows from the axisymmetric cylindrical geometry of the SECM.

As the UME tip approaches the Pd nanoparticle-decorated surface, the radical, $MV^{+\bullet}$, electro-generated at the UME, injects an electron into a Pd nanoparticle promoting the following overall reaction:

$$MV^{+\bullet} + H^+ \xrightarrow{\text{Pd nanoparticles}} MV^{2+} + \frac{1}{2}H_2 \quad (17)$$
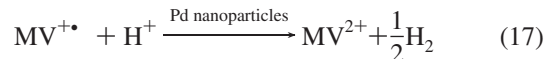
On the basis of the possible rate laws outlined in the previous section, we may write a general rate expression of the form[36]

$$\text{Rate} = k_{eff}c_{H^+}{}^x \exp\left(-\frac{\alpha nF}{RT}\eta\right) \quad (18)$$

where x is the reaction order with respect to H^+ ($n = 1$ is the number of electrons transferred) and k_{eff} is an effective rate constant, which will depend on the nanoparticle number density, Γ_{Pd} (cm^{-2}), as defined below. The formulation treats the substrate as uniform, which is reasonable given that the tip/substrate diffusion distance (micrometers) is orders of magnitude greater than the internanoparticle diffusion distance (ca. tens of nanometers).[49] Furthermore, the nanoparticles are assumed to be uniformly distributed over the surface, which is also reasonable. The true rate constant for the HER at the Pd nanoparticles, k_{part}, is related to the effective rate constant measured by SECM as

$$k_{part} = \frac{k_{eff}}{f} \quad (19)$$

where f is the fraction of the surface covered by Pd nanoparticles. The true rate constant for the HER at the Pd nanoparticles can further be extracted since

$$f = \Gamma_{Pd} \times A_{Pd} \quad (20)$$

where A_{Pd} is the effective single nanoparticle area ($A_{Pd} \sim \pi r_{Pd}^2$,[49] where r_{Pd} is the particle radius given that the particle is immobilized).

The overpotential for hydrogen evolution, η, is determined by the surface concentration ratio of the $MV^{2+/+\bullet}$ couple,[33,59]

$$\eta = E_{MV^{2+}/MV^{+\bullet}}^{0'} + \frac{RT}{F}\ln\left(\frac{[MV^{2+}]_{surface}}{[MV^{+\bullet}]_{surface}}\right) \quad (21)$$

where $E_{MV^{2+}/MV^{+\bullet}}^{0'}$ is the formal redox potential of the $MV^{2+/+\bullet}$ couple. We may write this expression because the $MV^{2+/+\bullet}$ couple is reversible while the HER is irreversible.[33,59] By combining eq 18 and eq 21, the reaction rate can be expressed by

$$\text{Rate} = k_{eff}c_{H^+}{}^x\left(\frac{[MV^{+\bullet}]_{surface}}{[MV^{2+}]_{surface}}\right)^\alpha \exp\left(-\frac{\alpha FE_{MV^{2+}/MV^{+\bullet}}^{0'}}{RT}\right) \quad (22)$$

In a particular experiment, Γ_{Pd} and the bulk value of c_{H^+} were fixed and the concentration of H^+ was such that it was not consumed appreciably. Thus, the boundary condition at the nanostructured interface can be written in terms of a phenomenological rate constant, k_{obs}:

$$D_{MV^{2+}}\frac{\partial c_{MV^{2+}}(r, z)}{\partial z}\bigg|_{z=d+\frac{a}{2}} = k_{obs}\left(\frac{[MV^{+\bullet}]_{surface}}{[MV^{2+}]_{surface}}\right)^\alpha \quad (23)$$

where

$$k_{obs} = k_{eff}c_{H^+}{}^x \exp\left(-\frac{\alpha FE_{MV^{2+}/MV^{+\bullet}}^{0'}}{RT}\right) =$$

$$k_{part}\Gamma_{Pd}A_{Pd}c_{H^+}{}^x$$

$$\exp\left(-\frac{\alpha FE_{MV^{2+}/MV^{+\bullet}}^{0'}}{RT}\right) \quad (24)$$

The mass transport problem outlined was modeled using a commercial finite element method modeling package (FEM-

LAB, Version 3.1), in conjunction with MATLAB (Version 7.1, Release 14). This was run on a Dell desktop PC running Windows XP with 1.5 GB RAM and a 2.52 GHz Pentium 4 Processor. The problem was solved in real space to allow direct analysis of the experimental data. The model yielded the steady-state tip current, i_t, which is normalized by the value with the probe UME in bulk solution, i_{bulk}, in the results which follow. The tip/substrate separation, d, has been normalized by the probe electrode base radius, a. It is important to note that k_{obs} and α were the only adjustable parameters involved in fitting experimental SECM approach curves and this allowed the various mechanistic cases to be readily distinguished.

4. Results and Discussion

4.1. Electrostatic Adsorption of Pd Nanoparticles. Electrostatic adsorption of colloids at polyelectrolyte films is a versatile approach for generating two-dimensional arrays with control over the particle number density.[47–52] Topographic AFM images of PLYS-treated mica surfaces for various Pd nanoparticle adsorption times are shown in Figure 2. Consistent with previous studies of other types of nanoparticles,[49] the electrostatic adsorption of citrate-stabilized Pd colloids on ultrathin PLYS film generates 2D arrays of monodisperse nanoparticles with a very low occurrence of aggregates on the time scale considered. It can be seen that a dense monolayer of nanoparticles [$\Gamma_{Pd} = (2.4 \pm 0.1) \times 10^{10}$ cm^{-2}] results after an adsorption time of 1 h. The nanoparticle number density, extracted from the analysis of the AFM images, as a function of the adsorption time, is illustrated in Figure 3. The adsorption kinetics can be phenomenologically rationalized in terms of a maximum number of adsorbed particles, $\Gamma_{Pd,max}$ and coverage independent rate constants for adsorption (k_a) and desorption (k_d),[49]

$$\Gamma_{Pd} = \Gamma_{Pd,max} \frac{k_a}{k_a + k_d} [1 - \exp(-(k_a + k_d)t)] \quad (25)$$

The dashed line in Figure 3 was obtained from fitting eq 25, taking the steady state value [$\Gamma_{Pd,max}(k_a/k_a + k_d)$] and ($k_a + k_d$)

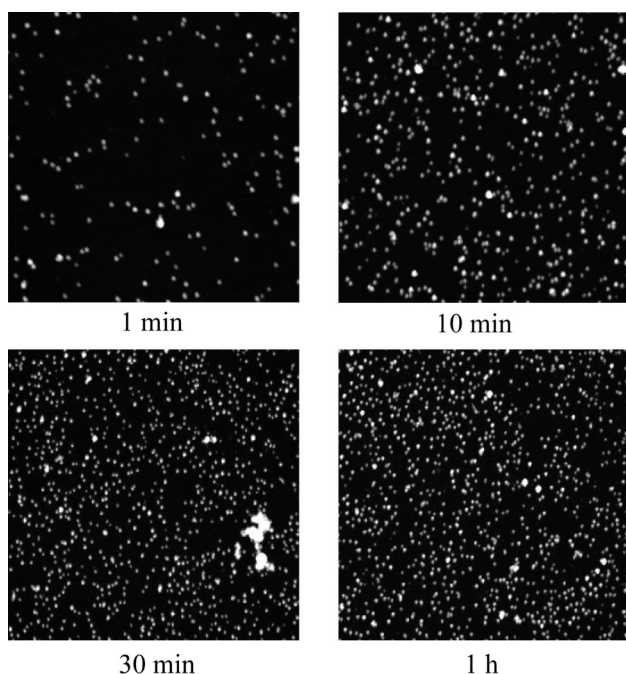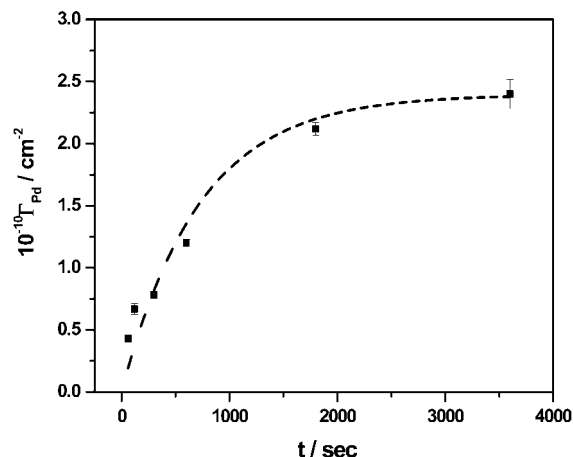**Figure 3.** Nanoparticle number density as a function of the adsorption time extracted from AFM measurements. The error bars result from the analysis of different samples with the same adsorption time. The dashed line corresponds to the fit to a model described by eq 25.
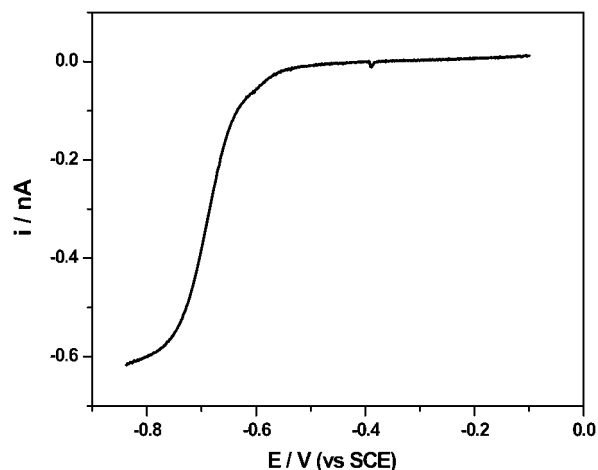

Figure 4. Linear sweep voltammogram for MV^{2+} reduction recorded at a 25 μm base diameter Au/Hg UME (vs SCE) in a pH 3 buffered solution containing 0.1 mM MV^{2+} and 0.05 M KNO$_3$. The scan rate was 20 mV s^{-1}.

as independent adjustable parameters. When one assumes that $k_a \gg k_d$, the data in Figure 3 yields values of $(2.4 \pm 0.2) \times 10^{10}$ cm^{-2} and $(1.4 \pm 0.3) \times 10^{-3}$ s^{-1} for $\Gamma_{Pd,max}$ and k_a, respectively. Previous studies employing Au nanoparticles with an average core diameter of 20 nm provided values within the same order of magnitude.[36]

4.2. SECM Approach Curve Measurements of the HER. In order to obtain quantitative information on the HER kinetics from the approach curves, the generation of the radical MV$^{+\bullet}$ from the reduction of MV^{2+} was set at the diffusion limit via the potential applied to the UME probe. A characteristic steady-state voltammogram for the reduction of MV^{2+} (0.1 mM) at a Au/Hg UME is shown in Figure 4. From the data, $E^{0'}_{MV^{2+}/MV^{+\bullet}}$ was evaluated as -0.68 V versus SCE, a parameter required for the estimation of the overpotential (see eq 21). The deposition of mercury on the Au electrode increases the overpotential for hydrogen evolution which would otherwise interfere in the analysis.

Approach curves measured against a PLYS-treated mica surface, as a function of Pd nanoparticle number density, are illustrated in Figure 5. The results show that as the nanoparticle surface coverage increases, the curves exhibit increasing positive feedback responses. As illustrated in Figure 1a, the positive feedback arises from the regeneration of MV^{2+} at the substrate

Figure 2. AFM images (2 μm × 2 μm) of Pd nanoparticles adsorbed on PLYS-treated mica as a function of the adsorption time (indicated in the figures).

Redox-Mediated Hydrogen Evolution
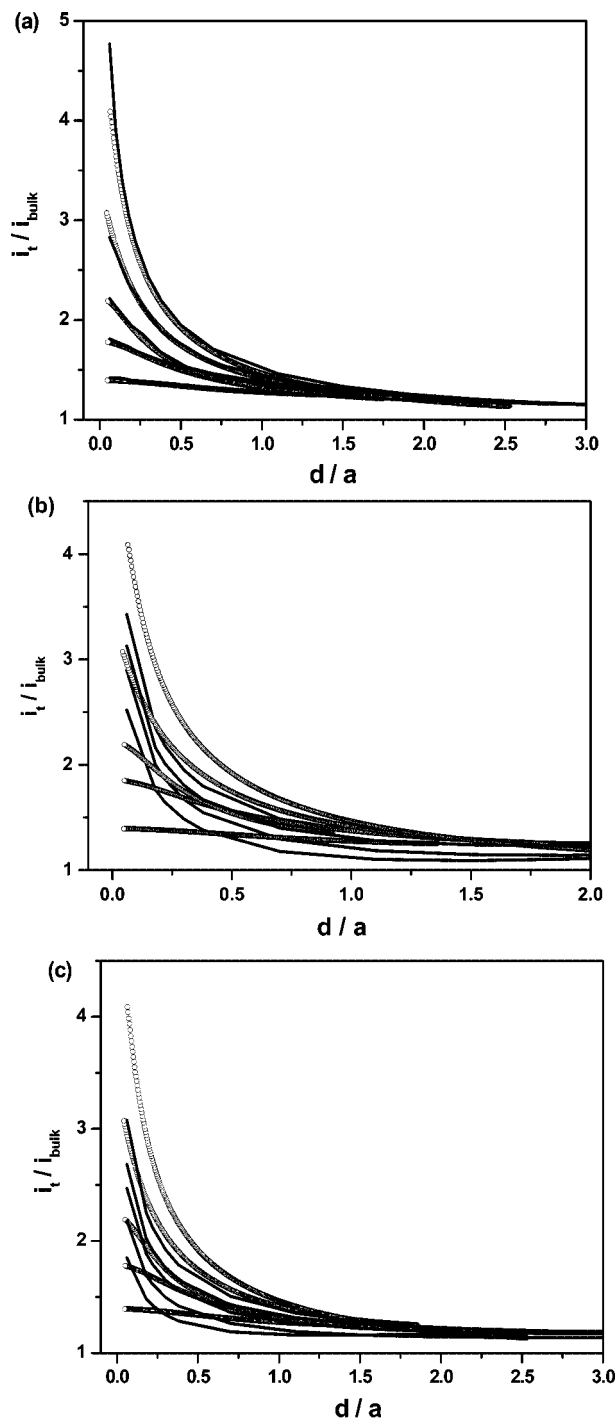
J. Phys. Chem. C, Vol. 112, No. 26, 2008 **9691**

Figure 5. Experimental (○) and simulated (solid curves) approach curves for PLYS-treated mica surfaces with adsorbed Pd nanoparticles in a pH 3 buffered solution containing 0.1 mM MV^{2+} and 0.05 M KNO_3 as a function of the nanoparticle number density. The best fits to simulated curves (solid lines) are for (a) $\alpha = 0.5$, (b) $\alpha = 1.5$, and (c) $\alpha = 2$. In all figures, from bottom to top, $\Gamma_{Pd} = (4.3 \pm 0.3) \times 10^9$, $(7.8 \pm 0.3) \times 10^9$, $(1.2 \pm 0.1) \times 10^{10}$, $(2.1 \pm 0.1) \times 10^{10}$ and $(2.4 \pm 0.1) \times 10^{10}$ cm^{-2}, respectively. In each plot, the highest curve solid line corresponds to diffusion-controlled positive feedback (fitted in a). In a, the remaining curves, from bottom to top, fit well to kinetic rate constants, k_{obs}, of 3.5×10^{-10}, 6.5×10^{-10}, 1.0×10^{-9}, and 2.0×10^{-9} mol cm^{-2} s^{-1}, respectively. In b, from bottom to top, the theoretical values of k_{obs} used to try and fit the experimental approach curves were 1.0×10^{-10}, 3.5×10^{-10}, 6.5×10^{-10}, and 2.0×10^{-9} mol cm^{-2} s^{-1}, respectively. In c, from bottom to top, the theoretical values of k_{obs} used to try and fit the experimental approach curves were 1.0×10^{-10}, 3.5×10^{-10}, 6.5×10^{-10}, 1.0×10^{-9}, and 2.0×10^{-9} mol cm^{-2} s^{-1}, respectively.
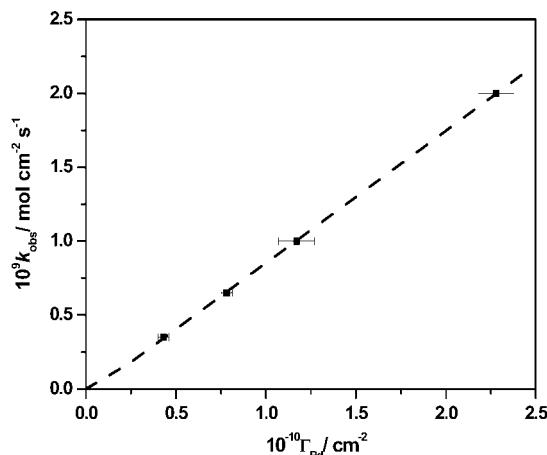

Figure 6. Apparent rate constants of the overall HER (k_{obs}) as a function of the Pd nanoparticle number density on PLYS-treated mica surfaces (Γ_{Pd}). The continuous line corresponds to the fit to eq 27.

because of the oxidation of $MV^{+\bullet}$ at the nanoparticle assembly. The rate of MV^{2+} regeneration is coupled to the rate of H^+ reduction at the nanoassembly as discussed above. As Γ_{Pd} increases, the flux of MV^{2+} from the substrate (eq 24) increases which manifests itself in a greater positive feedback current at the tip.

The experimental data were simulated with the SECM model in terms of the three values of α highlighted in the theory section. The continuous lines in Figure 5a–c correspond to the simulations taking the apparent transfer coefficient $\alpha = 0.5$, 1.5, and 2, respectively. The simulations clearly show that the distance-dependence of the current is significantly dependent on α. The curves in Figure 5 convincingly show that the simulations taking $\alpha = 0.5$ reproduce the experimental data most faithfully and the other α values do not fit the data. By considering the electrocatalytic behavior of extended Pd surfaces, this phenomenological transfer coefficient is consistent with the Volmer–Heyrovsky mechanism, that is, coupled discharge-electrodic-desorption (eq 1 and eq 3) as the most plausible mechanism at high overpotentials.[58] However, as highlighted earlier,[58] $\alpha = 0.5$ also describes a mechanism where the rate is controlled by the discharge step, independent of the nature of hydrogen recombination. These data are consistent with those of Stimming et al. who reported a similar potential-dependence for HER on Pd clusters deposited on Au (111).[20] However, they observed a gradually enhanced HER rate which was attributed to the spillover of adsorbed H atoms to the Au surface, accelerating the rate of desorption. On the other hand, Markovic et al. also observed a 120 mV/dec Tafel slopes on epitaxial Pd layers on Pt (111) electrodes at high overpotentials,[29] consistent with our work.

The rate of the HER at the nanostructured Pd surface may also be expressed in terms of the current density, j:

$$\text{Rate} = j/F = \Gamma_{Pd}A_{Pd}(j_0/F) \exp\left(-\frac{\alpha F}{RT}\eta\right) \quad (26)$$

where j_0 is the exchange current density per particle. For $\alpha = 0.5$,

$$k_{obs} = \Gamma_{Pd}A_{Pd}(j_0/F) \exp\left(-\frac{FE^{0'}_{MV^{2+}/MV^{+\bullet}}}{2RT}\right) \quad (27)$$

The values of k_{obs}, measured as a function of the nanoparticle number density on the substrate, from the simulation of approach curves in Figure 5a, are displayed in Figure 6. It is clear that

9692 *J. Phys. Chem. C, Vol. 112, No. 26, 2008*

Li et al.

k_{obs} increases linearly with increasing nanoparticle number density. Note that, at the highest nanoparticle number density considered (ca. $(2.4 \pm 0.1) \times 10^{10}$ cm^{-2}), the feedback curve became entirely dominated by diffusion of the MV$^{2+/+\bullet}$ couple in the tip/substrate gap (pure positive feedback[60]), so that it was not possible to extract a rate constant. In the figure, the linear relationship between k_{obs} and Γ_{Pd} with the intercept at the origin of the graph is not only consistent with eq 27, but also confirms that regeneration of MV^{2+} only occurs at the Pd nanoparticles. Taking $A_{Pd} = 1.33 \times 10^{-12}$ cm^2 ($A_{Pd} = \pi r_{Pd}^2$,[49] where r_{Pd} is the particle radius) and inputting $E^{0'}_{MV^{2+}/MV^{+\bullet}} = -0.44$ (vs NHE; obtained from the measured $E^{0'}_{MV^{2+}/MV^{+\bullet}} = -0.68$ V, vs SCE) into eq 27, the slope in Figure 6 allows estimation of the average exchange current density per particle at pH 3, $j_{0(pH = 3)} = (1.19 \pm 0.08) \times 10^{-6}$ A cm^{-2}. This value is comparable to the exchange current density quoted for bulk polycrystalline Pd. For instance, j_0 has been reported in the range of 6.3×10^{-2} to 2.0×10^{-4} at pH close to 0,[30a,61] which is the same order as our data, taking into account the dependence of the reaction rate on the pH of solution based on eq 22. This result suggests that citrate, which is weakly adsorbed on the nanoparticle surface, does not significantly inhibit the HER. Furthermore, the bulk-like catalytic behavior of the 13 nm diameter Pd particles is consistent with the partial occupancy of the d band for clusters of this dimension.[62] At first glance, this result may not appear consistent with the substantial enhancement of the electrocatalytic activity of nanoscopic Pd islands deposited on Au (111) electrodes reported by Stimming and co-workers.[20a] The key difference arises from the role played by the substrate in the interfacial reaction. As mentioned above, Padelov and Stimming recently concluded that hydrogen adsorbed on Pd spilled over the Au surface where rapid H$_2$ desorption occurred,[63] thus driving the reaction.

Experiments were conducted in buffer solution to avoid complications from the consumption of protons changing the proton concentration during an approach curve measurement. Although the MV^{2+} concentration was only 0.1 mM ($\sim$10% of the free proton concentration) and the diffusion coefficient of protons is approximately 1 order of magnitude higher than that of MV^{2+}, the redox mediator may undergo rapid diffusional feedback between the tip and the substrate (for fast substrate kinetics), whereas protons consumed in the HER are replenished by hindered diffusion into the substrate gap. For the lowest nanoparticle number densities, where the surface kinetics were slowest (and H$^+$ depletion minimal), we carried out control experiments with the solution at pH 3 with only free protons. Similar data were obtained and rate constants measured as outlined in Supporting Information, indicating that the buffer solution does not impact the observed kinetics.

4.3. Estimation of the Effective Overpotential at the Nanoparticle Assembly. Further analysis of the mechanism behind the HER requires knowledge of the local overpotential at the nanoparticle assembly. As shown below, simulations of the feedback current also allowed estimation of the concentration ratio of the redox probe at the substrate surface and the local overpotential.

Radial concentration profiles of MV^{2+} along the substrate surface plane ($[MV^{2+}]_{z=d+a/2,r}$) for different d are exemplified in Figure 7. These curves were calculated for $\Gamma_{Pd} = (4.3 \pm 0.3) \times 10^9$ cm^{-2} with kinetic and other parameters as outlined above. For the three d values considered, 18.75, 4.75, and 0.75 μm, $[MV^{2+}]_{z=d+a/2,r}$ exhibits a minimum at the position on the substrate directly beneath the center of the UME ($r = 0$). This result indicates that the overpotential for the HER is higher at
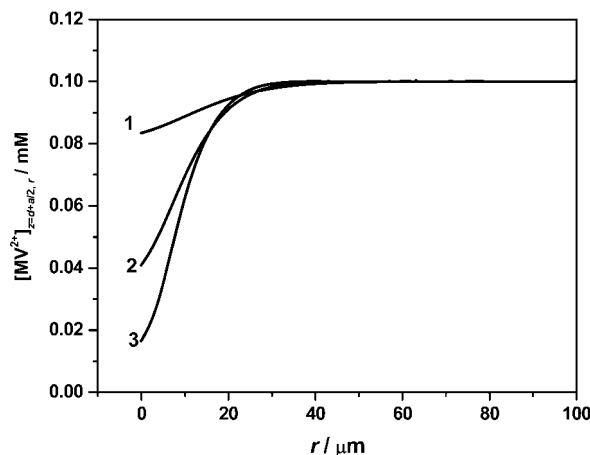

Figure 7. Calculated concentration profiles of MV^{2+} along the substrate surface plane ($[MV^{2+}]_{z=d+a/2,r}$) for three different UME/substrate separations d: 18.75 μm (curve 1), 4.75 μm (curve 2), and 0.75 μm (curve 3). The value of k_{obs} input into the model was 3.5×10^{-10} mol cm^{-2} s^{-1} with a typical value of $\Gamma_{Pd} = (4.3 \pm 0.3) \times 10^9$ cm^{-2} presenting the lowest surface density studied.

this point in the nanoparticle assembly. As r increases, $[MV^{2+}]_{z=d+a/2,r}$ gradually increases to the bulk value, 0.1 mM. The variation of the overpotential with r may aid mechanistic resolution between candidate cases. The theoretical treatment outlined considers a single value for the transfer coefficient and standard rate constant, which implies that over most of the range of interfacial potentials one mechanism should predominate. As highlighted below, for the situation herein, the reaction is driven and this assumption is reasonable.

It is also seen that as d decreases from 18.75 to 0.75 μm, $[MV^{2+}]_{z=d+a/2,r}$ at $r = 0$ decreases from 0.083 to 0.010 mM. This change in the concentration ratio of the redox probe reveals that the average potential at the nanoparticle assembly can be tuned with the position of the UME. It also explains why approach curves measurements are so sensitive to α, because, as the tip/substrate separation changes, the concentration ratio varies (for a kinetically limited situation) and so the driving force changes.

The concentration of MV$^{+\bullet}$ at a nanostructured interface ($[MV^{+\bullet}]_{z=d+a/2,r=0}$) can also be estimated from the simulation of the approach curves at various Γ_{Pd} as illustrated in Figure 8. In this figure, $[MV^{+\bullet}]_{z=d+a/2,r=0}$ was computed at $r = 0$ as a function of the normalized distance between the UME and the surface (d/a). As intuitively expected, for a given Γ_{Pd}, $[MV^{+\bullet}]_{z=d+a/2,r=0}$ increases; as the UME approaches the nanoparticle assembly, the mass transport rate increases and so the reaction becomes more kinetically limited. It follows that the distance-dependence of $[MV^{+\bullet}]_{z=d+a/2,r=0}$ is also rather sensitive to the nanoparticle number density, attaining highest values for smaller Γ_{Pd} because the net reaction flux sustained by the surface is lower. The corresponding overpotential for the HER at the nanoparticle surface can be estimated from the simulated surface concentration ratio of the MV$^{2+/+\bullet}$ couple based on eq 1. The result is that the overpotential shifts to more negative values with decreasing tip/substrate separation, due to the increase of $[MV^{+\bullet}]_{z=d+a/2,r=0}$ at closer distances. For the experiments herein, the HER overpotential is in excess of 250 mV as the tip approaches the surface. This significantly large value provides further support to the kinetic analysis that the coupled discharge-electrodic-desorption is the most plausible mechanism.[58]
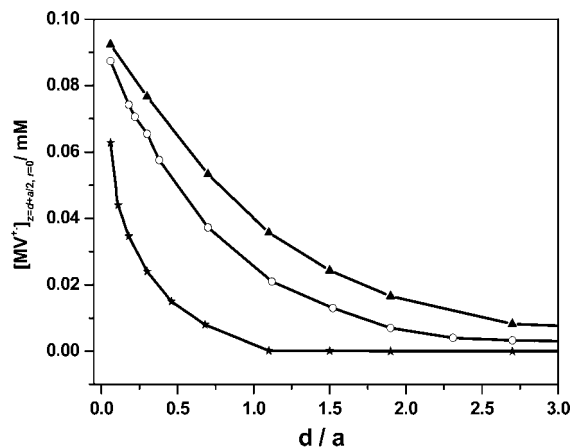
Redox-Mediated Hydrogen Evolution

J. Phys. Chem. C, Vol. 112, No. 26, 2008 **9693**

Figure 8. Calculated concentration profiles of $MV^{+\bullet}$ at a nanostructured surface ($[MV^{+\bullet}]_{z=d+a/2, r=0}$) as a function of d/a at different nanoparticle number densities: -▲- $\Gamma_{Pd} = (4.3 \pm 0.3) \times 10^9$ cm^{-2}; -O- $\Gamma_{Pd} = (7.8 \pm 0.3) \times 10^9$ cm^{-2}; and -*- $\Gamma_{Pd} = (2.1 \pm 0.1) \times 10^{10}$ cm^{-2}. The values of k_{obs} input into the model for different particle number densities were 3.5×10^{-10}, 6.5×10^{-10}, and 2.0×10^{-9} mol cm^{-2} s^{-1}, respectively.

5. Conclusions

The dynamics of the HER at two-dimensional assemblies of Pd nanoparticles has been investigated using SECM. Control over the nanoparticle adsorption time allowed the nanoparticle number density at the surface to be varied in a well-defined way. In the SECM approach, the Fermi level of the nanoparticles is controlled by the concentration ratio of the methyl viologen couple at the substrate which depends on the UME/substrate separation, HER kinetics, particle density and bulk concentration of MV^{2+}. Analysis of the approach curves allowed estimation of the average exchange current density for single Pd particles. This was comparable to bulk Pd, which is consistent with the bulk-like electronic structure of particles of this size. Significantly, quantitative analysis of the SECM approach curves resulted in a phenomenological electron transfer coefficient of 0.5. This value is consistent with the Volmer−Heyrovsky model, with coupled discharge-electrodic-desorption as the most plausible mechanism at high overpotentials.

In contrast to conventional electrochemical approaches, the methodology described herein allows intrinsic nanoparticle reactivity to be investigated free from electronic and structural effects induced by the electrode substrate. This issue is particularly relevant for uncoupling size-dependent reactivity of clusters from the effect of cluster−substrate interactions, which we will explore in future work. Recent discussions on the catalytic properties of Pd nanotructures electrodeposited on Au substrates illustrate the complexity of this system.[6,20,32] From the practical point of view, implementing this approach in the SECM configuration opens up the possibility of mapping the surface reactivity of heterogeneous catalysts for hydrogenation at higher resolution. In future work, we plan to use this method to access the properties of other nanostructured catalysts and interfaces.

References and Notes

(1) Bockris, J. B. *J. Phys. Chem.* **1958**, *62*, 766.

(2) Kiwi, J.; Gratzel, M. *Nature* **1979**, *281*, 657.

(3) Ohms, D.; Plzak, V.; Trasatti, S.; Wiesener, K.; Wendt, H. In *Electrochemical Hydrogen Technologies*; Wendt, H., Ed.; Elsevier: Amsterdam, 1990; pp 1−4..

(4) Mizuno, T.; Enyo, M. *Modern Aspects of Electrochemistry*; Plenum: New York, 1996; Vol. *30*, p 415.

(5) Grass, V.; Lexa, D.; Saveant, J. M. *J. Am. Chem. Soc.* **1997**, *119*, 7526.

(6) Meier, J.; Schiotz, J.; Liu, P.; Nørskov, J. K.; Stimming, U. *Chem. Phys. Lett.* **2004**, *390*, 440.

(7) Hinnemann, B.; Moses, P. G.; Bonde, J.; Jorgensen, K. P.; Nielsen, J. H.; Horch, S.; Chorkendorff, I.; Nørskov, J. K. *J. Am. Chem. Soc.* **2005**, *127*, 5308.

(8) Goltsov, V. A.; Veziroglu, T. N.; Goltsova, L. F. *Int. J. Hyd. En.* **2006**, *31*, 153.

(9) Kibler, L. A. *Chem. Phys. Chem.* **2006**, *7*, 985.

(10) Jaramillo, T. F.; Jørgensen, K. P.; Bonde, J.; Nielsen, J. H.; Horch, S.; Chorkendorff, I. *Science* **2007**, *317*, 100.

(11) Trasatti S. In *Advances in Electrochemical Science and Engineering*; Gerischer, H., Tobias, C. W., Eds.; VCH−Weinhem: New York; 1992, pp 1−85.

(12) Guo, Y. Z.; Guadalupe, A. R. *Langmuir* **1999**, *15*, 759.

(13) Zhang, Y. R.; Asahina, S.; Yoshihara, S.; Shirakashi, T. *Electrochim. Acta* **2003**, *48*, 741.

(14) Jin, Y. D.; Shen, Y.; Dong, S. J. *J. Phys. Chem. B* **2004**, *108*, 8142.

(15) (a) Day, T. M.; Unwin, P. R; Wilson, N. R; Macpherson, J. V. *J. Am. Chem. Soc.* **2005**, *127*, 10639. (b) Day, T. M.; Unwin, P. R.; Macpherson, J. V. *Nano Lett.* **2007**, *7*, 51.

(16) Stott, S. J.; Mortimer, R. J.; Dann, S. E.; Oyama, M.; Marken, F. *Phys. Chem. Chem. Phys.* **2006**, *8*, 5437.

(17) Feldheim, D. L. *Science* **2007**, *316*, 699.

(18) Estephan, Z. G.; Alawieh, L.; Halaoui, L. I. *J. Phys. Chem. C* **2007**, *111*, 8060.

(19) (a) Tian, N.; Zhou, Z.-Y.; Sun, S.-G.; Ding, Y.; Wang, Z.-L. *Science* **2007**, *316*, 732. (b) Zhang, J.; Sasaki, K.; Sutter, E.; Adzic, R. R. *Science* **2007**, *315*, 220. (c) Valden, M.; Lai, X.; Goodman, W. D. *Science* **1998**, *281*, 1647.

(20) (a) Meier, J.; Friedrich, K. A.; Stimming, U. *Faraday Discuss.* **2002**, *121*, 365. (b) Eikerling, M.; Meier, J.; Stimming, U. *Z. Phys. Chem.* **2003**, *217*, 395.

(21) Qian, D. J.; Wakayama, T.; Nakamura, C.; Miyake, J. *J. Phys. Chem. B* **2003**, *107*, 3333.

(22) Beck, A.; Horváth, A.; Sárkány, A.; Guczi, L. In *Nanotechnology in Catalysis*; Zhou, B.; Hermans, S.; Somorjai, G. A. Eds; Springer, 2004, vol. 1, ch. 5, pp 83−106.

(23) Bertoncello, P.; Peruffo, M.; Unwin, P. R. *Chem. Commun.* **2007**, 1597.

(24) Saraby-Reintjes, A. *Electrochim. Acta* **1986**, *31*, 251.

(25) Fournier, J.; Wrona, P. K.; Lasia, A.; Lacasse, R.; Lalancette, J; Menard, H.; Brossard, L. *J. Electrochem. Soc.* **1992**, *139*, 2372.

(26) Dabo, P.; Brossard, L.; Menard, H. J. *Electrochem. Soc.* **1998**, *145*, 3150.

(27) Pozio, A.; Giorgi, L.; Antolini, E.; Passalacqua, E. *Electrochim. Acta* **2000**, *46*, 555.

(28) Giorgi, L.; Pozio, A.; Bracchini, C.; Giorgi, R.; Turtu, S. *J. Appl. Electrochem.* **2001**, *31*, 325.

(29) Markovic, N. M.; Lucas, C. A.; Climent, V.; Stamenkovic, V.; Ross, P. N. *Surf. Sci.* **2000**, *465*, 103.

(30) (a) Nørskov, J. K.; Bligaard, T.; Logadottir, A.; Kitchin, J. R.; Chen, J. G.; Pandelov, S.; Stimming, U. *J. Electrochem. Soc.* **2005**, *152*, J23. (b) Greely, J.; Jaramillo, T. F.; Bonde, J.; Chorkendorff, I.; Nørskov, J. K. *Nat. Mater.* **2006**, *5*, 909.

(31) Schmickler, W.; Trasatti, S. *J. Electrochem. Soc.* **2006**, *152*, L31.

(32) Sanchez, C. G.; Leiva, E. P. M.; Schmickler, W. *Electrochem. Commun.* **2003**, *5*, 584.

(33) Selzer, Y.; Turyan, I.; Mandler, D. *J. Phys. Chem. B* **1999**, *103*, 1509.

(34) hou, J. F.; Zu, Y. B.; Bard, A. J. *J. Electroanal. Chem.* **2000**, *491*, 22.

(35) Jayaraman, S.; Hillier, A. C. *Langmuir* **2001**, *17*, 7857.

(36) Zhang, J.; Lahtinen, R. M.; Kontturi, K.; Unwin, P. R.; Schiffrin, D. J. *Chem. Commun.* **2001**, 1818.

(37) Jambunathan, K; Hillier, A. C. *J. Electroanal. Chem.* **2002**, *144*, 524.

(38) Zoski, C. G. *J. Phys. Chem. B* **2003**, *107*, 6401.

(39) Fernandez, J. L.; Walsh, D. A.; Bard, A. J. *J. Am. Chem. Soc.* **2005**, *127*, 357.

(40) Eckhard, K.; Chen, X. X.; Turcu, F.; Schuhmann, W. *Phys. Chem. Chem. Phys.* **2006**, *8*, 5359.

(41) Bard, A. J., Mirkin, M. V., Eds. *Scanning Electrochemical Microscopy*, Marcel Dekker: New York, 2001.

(42) Quinn, B. M.; Liljeroth, P.; Kontturi, K. *J. Am. Chem. Soc.* **2002**, *124*, 12915.

(43) Ruiz, V.; Liljeroth, P.; Quinn, B. M.; Kontturi, K. *Nano Lett.* **2003**, *3*, 1459.

(44) Georganopoulou, D. G.; Mirkin, M. V.; Murray, R. W. *Nano Lett.* **2004**, *4*, 1763.

(45) Carano, M.; Lion, N.; Abid, J. P.; Girault, H. H. *Electrochem. Commun.* **2004**, *6*, 1217.

(46) Xiong, H.; Gross, D. A.; Guo, J. D.; Amemiya, S. *Anal. Chem.* **2006**, *78*, 1946.

(47) Kakkassery, J. J.; Abid, J.-P.; Carrara, M.; Fermin, D. J. *Faraday Discuss.* **2004**, *125*, 157.

(48) Bergkvist, M.; Mark, S. S.; Yang, X.; Angert, E. R.; Batt, C. A. *J. Phys. Chem. B* **2004**, *108*, 8241.

(49) Zhao, J. J.; Bradbury, C. R.; Huclova, S.; Potapova, I.; Carrara, M.; Fermin, D. J. *J. Phys. Chem. B* **2005**, *109*, 22985.

(50) Zhang, H.; Lu, H. Y.; Hu, N. F. *J. Phys. Chem. B* **2006**, *110*, 2171.

(51) Carrara, M; Kakkassery, J. J.; Abid, J.-P.; Fermin, D. J. *Chem. Phys. Chem.* **2004**, *5*, 571.

(52) Schnippering, M.; Carrara, M.; Foelske, A.; Kötz, R.; Fermin, D. J. *Phys. Chem. Chem. Phys.* **2007**, *9*, 725.

(53) Turkevich, J.; Miner, R. S.Jr.; Babenkova, L. *J. Phys. Chem.* **1986**, *90*, 4765.

(54) Ciani, I.; Burt, D. P.; Daniele, S.; Unwin, P. R. *J. Phys. Chem. B* **2004**, *108*, 3801.

(55) Mauzeroll, J.; Hueske, E. A.; Bard, A. J. *Anal. Chem.* **2003**, *75*, 3880.

(56) Slevin, C. J.; Macpherson, J. V.; Unwin, P. R. *J. Phys. Chem. B* **1997**, *101*, 10851.

(57) (a) Ruiz, V.; Nicholson, P. G.; Jollands, S.; Thomas, P. A.; Macpherson, J. V.; Unwin, P. R. *J. Phys. Chem. B* **2005**, *109*, 19335. (b) Nicholson, P. G.; Ruiz, V.; Macpherson, J. V.; Unwin, P. R. *Phys. Chem. Chem. Phys.* **2006**, *8*, 5096.

(58) Bockris, J. O'M.; Reddy, A. K. N. *Modern Electrochemistry*; Macdonald: London, 1970; Vol. 2, pp 1231−1251.

(59) Mills, A.; Douglas, P.; Russell, T. *J. Chem. Soc., Faraday Trans.* **1990**, *86*, 1417.

(60) Bard, A. J.; Fan, R. F.; Kwak, J.; Lev, O. *Anal. Chem.* **1989**, *61*, 132.

(61) Trasatti, S. *J. Electroanal. Chem.* **1972**, *39*, 163.

(62) Wertheim, G. K.; DiCenzo, S. B; Buchanan, D. N. E. *Phys. Rev. B* **1986**, *33*, 5384.

(63) Pandelov, S.; Stimming, U. *Electrochim. Acta* **2007**, *52*, 5548.